



# Distinct photocatalytic charges separation pathway on CuO<sub>x</sub> modified rutile and anatase TiO<sub>2</sub> under visible light

Min Chen<sup>a</sup>, Jianhua Chen<sup>b,c</sup>, Chuncheng Chen<sup>b,c,\*</sup>, Changbin Zhang<sup>a,c,\*</sup>, Hong He<sup>a,c</sup>

<sup>a</sup> State Key Joint Laboratory of Environment Simulation and Pollution Control, Research Center for Eco-Environment Sciences, Chinese Academy of Sciences, Beijing 100085, PR China

<sup>b</sup> Key Laboratory of Photochemistry, CAS Research/Education Center for Excellence in Molecular Sciences, Institute of Chemistry, Chinese Academy of Sciences, Beijing 100190, PR China

<sup>c</sup> University of Chinese Academy of Sciences, Beijing 100049, PR China

## ARTICLE INFO

### Keywords:

Anatase  
Rutile  
Cu  
Charge migration

## ABSTRACT

Modification of TiO<sub>2</sub> with copper oxides clusters (CuO<sub>x</sub>-TiO<sub>2</sub>) induces visible-light absorption and enhances its activity. In this work, we investigated the CuO<sub>x</sub>-anatase and CuO<sub>x</sub>-rutile for the photocatalytic oxidation of gaseous NH<sub>3</sub> under visible light. In contrast with the widely reported results that CuO<sub>x</sub>-anatase displays higher performance than CuO<sub>x</sub>-rutile in photocatalytic oxidation or reduction, we surprisingly observed that CuO<sub>x</sub>-rutile is able to oxidize NH<sub>3</sub> efficiently under visible light irradiation, while CuO<sub>x</sub>-anatase shows no activity. Further characterizations showed that visible-light inclines to drive the VB electrons of rutile TiO<sub>2</sub> to CuO<sub>x</sub> at the interface between rutile TiO<sub>2</sub> and CuO<sub>x</sub>, while it drives the electrons of CuO<sub>x</sub> to anatase TiO<sub>2</sub> at interface between anatase TiO<sub>2</sub> and CuO<sub>x</sub>. DFT calculations revealed that the interaction between CuO<sub>x</sub> and TiO<sub>2</sub> is markedly different in CuO<sub>x</sub>-anatase and CuO<sub>x</sub>-rutile, which induces the differences in the electronic distribution of interfacial Cu, O and Ti atoms, resulting in the distinct direction of charge transfer.

## 1. Introduction

TiO<sub>2</sub> is well-known as an efficient photocatalyst, and TiO<sub>2</sub> with different crystalline forms (anatase and rutile) is widely employed to various photocatalytic reactions [1–4]. Owing to the wide band gap, TiO<sub>2</sub> can be only activated under ultraviolet (UV) light irradiation, which limits its practical applications. Nano-copper oxide clusters (CuO<sub>x</sub>) grafting is recently shown to be a promising way to expand the visible-light photocatalytic activity of rutile and anatase TiO<sub>2</sub> [5–9]. The CuO<sub>x</sub>-TiO<sub>2</sub> has been investigated in many photocatalytic oxidation or reduction, such as degradation of organic pollutants, H<sub>2</sub> evolution, CO<sub>2</sub> reduction, etc. [5–10]. Anatase TiO<sub>2</sub> usually has the higher photocatalytic activity under illumination of UV light compared with rutile TiO<sub>2</sub> due to the wider bandgap and higher surface area [11,12]. Similarly, CuO<sub>x</sub>-anatase has also demonstrated the higher activity under UV and visible light compared with CuO<sub>x</sub>-rutile [6,10].

On the surface of CuO<sub>x</sub>-TiO<sub>2</sub>, the photocatalytic reactions are driven by visible-light induced interfacial charge transfer (IFCT) process between CuO<sub>x</sub> and TiO<sub>2</sub> [13–15]. Since TiO<sub>2</sub> itself cannot be directly excited by visible light, the electron is usually considered to be excited

from the valence band (VB) to conduction band (CB) of CuO<sub>x</sub>, and next transfers to the CB of TiO<sub>2</sub>, leading to the charge separation [16,17]. Similar scheme was also reported in TiO<sub>2</sub>-based heterojunctions, such as CdS-TiO<sub>2</sub>, g-C<sub>3</sub>N<sub>4</sub>-TiO<sub>2</sub>, and plasmonic metal-TiO<sub>2</sub> [18,19]. In contrast, several reports have shown that the direct excitation from the VB of TiO<sub>2</sub> to the metal species might occur under visible-light irradiation in the metal-grafted TiO<sub>2</sub> [8,13,17]. Hashimoto et al. reveal that the electrons in the valence band (VB) of rutile phase TiO<sub>2</sub> are excited and migrate to MO<sub>x</sub> (for example, CuO<sub>x</sub> and FeO<sub>x</sub>) through the interface between TiO<sub>2</sub> and MO<sub>x</sub> [13]. It is further supported by detecting reaction intermediates, such as trapped holes, trapped electrons, ·O<sub>2</sub><sup>-</sup>, and H<sub>2</sub>O<sub>2</sub> [16]. Thus, the direction of the charge migration between CuO<sub>x</sub> and TiO<sub>2</sub> is relatively complicated and a further investigation is greatly needed.

In above-mentioned two cases, the generated hole is left in the VB of CuO<sub>x</sub> or TiO<sub>2</sub>, and the disagreement about the direction of the charge migration on MO<sub>x</sub>-TiO<sub>2</sub> should be mainly due to the discrepancy in understanding the origin of the holes. Hence, confirming the location of hole will contribute to the better understanding of charge separation mechanism in CuO<sub>x</sub>-TiO<sub>2</sub>. Researches usually use decomposition of

\* Corresponding authors at: University of Chinese Academy of Sciences, Beijing 100049, PR China.

E-mail addresses: [ccchen@iccas.ac.cn](mailto:ccchen@iccas.ac.cn) (C. Chen), [cbzhang@reeces.ac.cn](mailto:cbzhang@reeces.ac.cn) (C. Zhang).

<https://doi.org/10.1016/j.apcatb.2021.120735>

Received 9 July 2021; Received in revised form 3 September 2021; Accepted 16 September 2021

Available online 20 September 2021

0926-3373/© 2021 Elsevier B.V. All rights reserved.

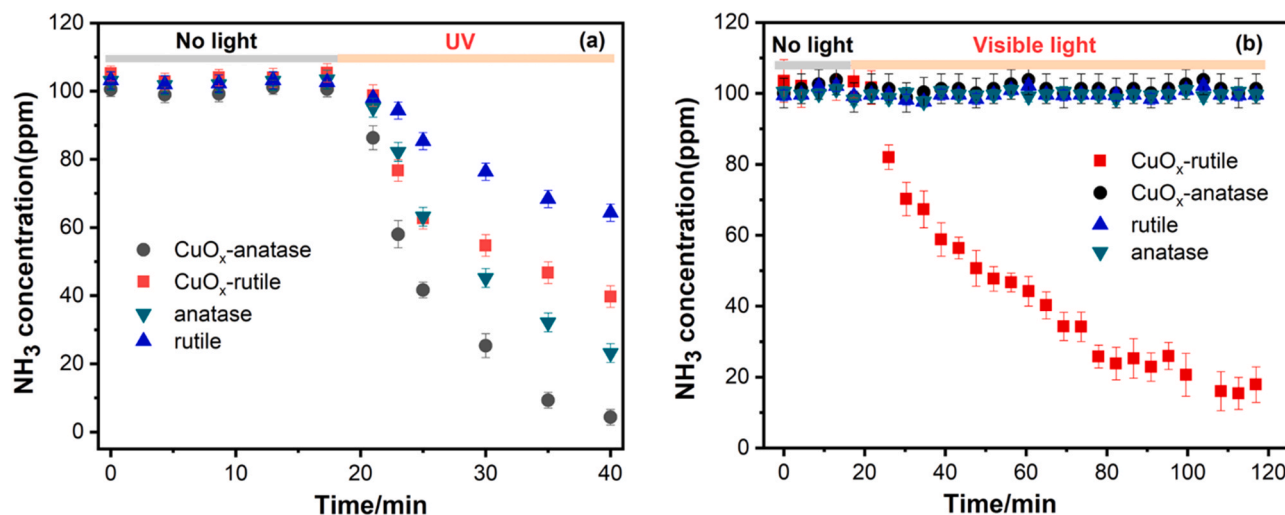


Fig. 1. Photocatalytic oxidation of NH<sub>3</sub> under UV (a) and visible light (b) over different samples. (100 ppm NH<sub>3</sub>, 20 vol% O<sub>2</sub>, RH 50% and N<sub>2</sub> balance).

model organic pollutants to judge the efficiency of MO<sub>x</sub>-TiO<sub>2</sub> [20]. The reported CuO<sub>x</sub>-TiO<sub>2</sub> or FeO<sub>x</sub>-TiO<sub>2</sub> shows excellent activities for oxidation of acetone and degradation of 2-naphthol or other dyes [16,21]. Since the active species such as holes, electrons, ·O<sub>2</sub><sup>-</sup>, and ·OH are all involved in these reactions, the specific role and source of the hole cannot be determined. Therefore, it is reasonable to propose that a typical oxidation reaction, which is very sensitive to the VB position of a photocatalyst, might be more suitable for effectively investigating the direction of charge migration on MO<sub>x</sub>-TiO<sub>2</sub>.

Recently, we demonstrated that TiO<sub>2</sub>-based hole is the key active species for the oxidation of NH<sub>3</sub> on TiO<sub>2</sub>-based photocatalysts, and therefore NH<sub>3</sub> activation can be a good indicator for the presence of TiO<sub>2</sub>-based hole [22–24]. In this study, we prepared the CuO<sub>x</sub>-grafted rutile and anatase TiO<sub>2</sub> catalysts, and carefully investigated the impact of TiO<sub>2</sub> crystalline structures on the charge migration mechanism of CuO<sub>x</sub>-TiO<sub>2</sub> by using a hole position sensitive NH<sub>3</sub> oxidation probe reaction, combining with EPR experiments and DFT calculations. We found that the charge migration pathway of CuO<sub>x</sub>-TiO<sub>2</sub> is closely dependent on the crystalline structures of TiO<sub>2</sub>, in which at the interface between rutile TiO<sub>2</sub> and CuO<sub>x</sub>, visible light drives the VB electrons of rutile TiO<sub>2</sub> to CuO<sub>x</sub>, while in case of the interface between anatase TiO<sub>2</sub> and CuO<sub>x</sub>, visible light is inclined to drive the excitation of CuO<sub>x</sub>, and the photoexcited electrons transfer to anatase TiO<sub>2</sub>. Our findings about the IFCT process between CuO<sub>x</sub>-TiO<sub>2</sub> will be very helpful for the deep understanding of the mechanism of charge migration in MO<sub>x</sub>-TiO<sub>2</sub>.

## 2. Experiment

### 2.1. Synthesis of catalysts

TiO<sub>2</sub> with different crystalline (anatase and rutile) was purchased from Aladdin. 1.0 g anatase or rutile TiO<sub>2</sub> nanoparticles were dispersed into the CuSO<sub>4</sub> aqueous solution. The amount of Cu<sup>2+</sup> relative to the amount of TiO<sub>2</sub> sample was 0.3 wt%. The dispersing solution under stirring was placed into a water-bath kept at 70 °C for 1 h. The obtained precipitates were washed with deionized water several times and then were dried in an oven at 70 °C for 24 h.

### 2.2. Activity tests

The activity tests for NH<sub>3</sub> oxidation were performed at room temperature in a flow reactor. 0.1 g of photocatalyst powders in a round dish was placed in the center of the reactor. The light source was a 500 W commercial Xe lamp (Beijing TrusTech Science and Technology Co.,

China). The concentrations of NH<sub>3</sub>, NO<sub>x</sub> (NO, NO<sub>2</sub>) and N<sub>2</sub>O were simultaneously measured by an online FTIR (Nicolet IS50) equipped with 2 m gas cell and a DTGS detector, and N<sub>2</sub> selectivity was calculated according to the N element balance by the following equations: N<sub>2</sub> selectivity = ([NH<sub>3</sub>]<sub>in</sub> - [NO<sub>x</sub>]<sub>out</sub> - 2[N<sub>2</sub>O]<sub>out</sub>) / [NH<sub>3</sub>]<sub>in</sub>. The reactant gas was 100 ppm NH<sub>3</sub>, 20 vol% O<sub>2</sub>, RH 50% and N<sub>2</sub> balance. The volume of reactant gas was about 1.5 L.

### 2.3. Characterization methods

Powder X-ray diffraction (XRD) measurements were performed on a X'Pert PRO MPD X-ray powder diffractometer (Japan) over the 2θ range from 10° to 90° with a scan step size of 0.02°. Transmission electron microscopy (TEM) images of the samples were taken on a JEOL 2100F instrument operating at an accelerating voltage of 200 kV. The UV–vis diffuse reflection spectra (DRS) were tested with UV–vis spectrophotometer (U-3310, Hitachi) using Al<sub>2</sub>O<sub>3</sub> as a reference. The X-band electron paramagnetic resonance (EPR) spectra were measured at 90 K using a Bruker E500 EPR spectrometer. The photoelectrochemical measurements were conducted on CHI 630B workstation and a saturated Ag/AgCl electrode and a platinum plate were used as the reference electrode and the counter electrode, respectively.

### 2.4. Computational methods

The calculations about interaction of CuO<sub>x</sub> with the (101) surfaces of anatase or (110) surface of rutile TiO<sub>2</sub> was performed with code VASP. The Perdew-Burke-Ernzerhof (PBE) GGA exchange-correlation functional was applied. A periodic slab with 2 × 2 surface unit cells for (101) surface of anatase TiO<sub>2</sub> and (101) surface of rutile TiO<sub>2</sub> was used. The models contain 108 atoms for (101) facets of anatase TiO<sub>2</sub> and 108 atoms for (110) facets of rutile TiO<sub>2</sub>. The bottom two layers of Ti and O were fixed in the process of structure optimization. The vacuum gap thickness was 15 Å. Gamma centered k-point meshes of 2 × 2 × 1 were employed. Structures were relaxed until the forces acting on each atom were smaller than 0.02 eV/Å.

## 3. Results and discussion

### 3.1. Activity tests for photocatalytic oxidation of NH<sub>3</sub>

The photocatalytic activity for oxidation of NH<sub>3</sub> was firstly tested. As shown in Fig. 1, under UV irradiation, both CuO<sub>x</sub>-anatase and CuO<sub>x</sub>-rutile show much higher activity compared with pure anatase and rutile

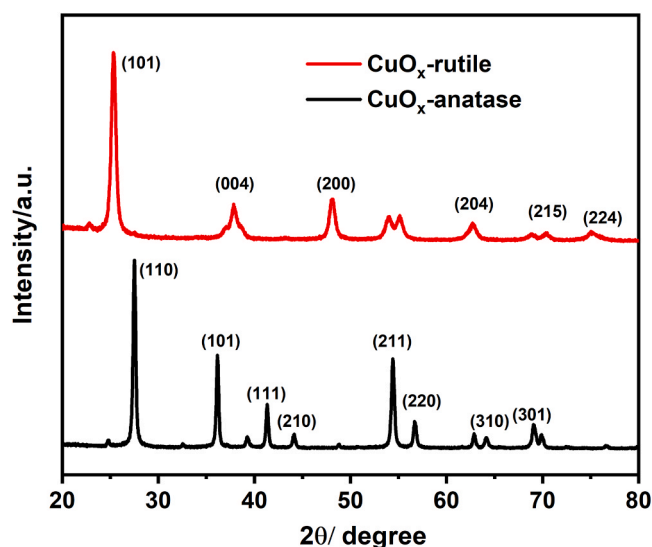


Fig. 2. X-ray diffraction pattern of CuO<sub>x</sub>-rutile and CuO<sub>x</sub>-anatase.

TiO<sub>2</sub>. The CuO<sub>x</sub>-anatase is more active than CuO<sub>x</sub>-rutile under UV light irradiation (Fig. 1a), and the NH<sub>3</sub> conversion over CuO<sub>x</sub>-anatase can reach above 95% in 20 min, while only 60% over CuO<sub>x</sub>-rutile. Notably, in the case of visible light irradiation, we surprisingly observed a completely different activity order between CuO<sub>x</sub>-rutile and CuO<sub>x</sub>-anatase, relative to that of under UV irradiation. The CuO<sub>x</sub>-rutile exhibits excellent performance towards NH<sub>3</sub> oxidation, while no any NH<sub>3</sub> conversion is observed at all on CuO<sub>x</sub>-anatase (Fig. 1b). We have measured the produced NO<sub>x</sub> and N<sub>2</sub>O during the reaction over CuO<sub>x</sub>-rutile under visible light and the results are presented in Fig. S1. It is shown that no NO and NO<sub>2</sub> was detected and about 12 ppm N<sub>2</sub>O is produced, and hence the selectivity of NH<sub>3</sub> to N<sub>2</sub> was calculated to be about 76%. The influences of Cu precursor, Cu loading amount and calcination temperature on the activities of CuO<sub>x</sub>-rutile were also investigated (Figs. S2–S4). It is shown that the optimal loading of Cu is 0.3 wt%, and the counterions of the Cu precursors such as chlorine, nitrate and sulfate have no clear impacts on the activity. The drastic different performances between CuO<sub>x</sub>-rutile and CuO<sub>x</sub>-anatase strongly indicates that there is a distinct mechanism of charge migration on CuO<sub>x</sub>-rutile and CuO<sub>x</sub>-anatase under visible light irradiation.

### 3.2. Structural characterizations

The structure of CuO<sub>x</sub>-rutile and CuO<sub>x</sub>-anatase were next investigated. X-ray diffraction (XRD) analysis shows that CuO<sub>x</sub>-anatase and CuO<sub>x</sub>-rutile contain the typical anatase and rutile crystalline phases, respectively (Fig. 2). The TEM images display that the CuO<sub>x</sub> clusters are uniformly distributed on rutile or anatase TiO<sub>2</sub>, and the sizes of the CuO<sub>x</sub> clusters in both samples are approximately 1–2 nm (Fig. 3). XPS analysis was employed to further detect the chemical states of the surface CuO<sub>x</sub>. As shown in Fig. S5, both CuO<sub>x</sub>-anatase and CuO<sub>x</sub>-rutile exhibit two peaks of Cu 2p<sub>1/2</sub> (952.9 eV) and Cu 2p<sub>3/2</sub> (933.1 eV), which are assigned to Cu<sup>2+</sup> [5,25]. We further conducted an EPR experiment to explore the chemical state of CuO<sub>x</sub>. The EPR signal with the g factor of 2.394 is dominant on CuO<sub>x</sub>-anatase and CuO<sub>x</sub>-rutile (Fig. S6), and this signal is ascribed to Cu<sup>2+</sup> species. Thus, the formed amorphous CuO<sub>x</sub> mainly exhibits the state of Cu (II), which is well consistent with the results previously reported [26,27]. Furthermore, the Cu 2p XPS spectra of the CuO<sub>x</sub>-rutile and CuO<sub>x</sub>-anatase after reaction were also measured. As shown in Figs. S7 and S8, the CuO<sub>x</sub> species remained in Cu<sup>2+</sup> state on the tested samples, indicating that the chemical properties of CuO<sub>x</sub> do not change after reaction.

### 3.3. Photo-electrochemical measurement

The UV–vis diffuse reflectance spectra (DRS) of the rutile TiO<sub>2</sub>, CuO<sub>x</sub>-rutile, anatase TiO<sub>2</sub> and CuO<sub>x</sub>-anatase samples were measured and compared, and the spectra are displayed in Fig. S9. The pristine rutile and anatase TiO<sub>2</sub> show no obvious visible light absorption. After the CuO<sub>x</sub> species are grafted, the absorption intensities of both CuO<sub>x</sub>-rutile and CuO<sub>x</sub>-anatase are increased in the visible light range, indicating that CuO<sub>x</sub> clusters on rutile or anatase TiO<sub>2</sub> introduce visible light absorption. To show the origin of the visible light absorption, we further compared the UV–vis diffuse reflectance spectra of CuO<sub>x</sub>-rutile and CuO<sub>x</sub>-anatase with rutile and anatase TiO<sub>2</sub> as background, respectively. As shown in Fig. 4, CuO<sub>x</sub>-rutile has strong absorption in 420–500 nm with a maximum at around 475 nm and 700–800 nm in visible light region, however, the dominant absorption of CuO<sub>x</sub>-anatase in visible light region is in the range of 700–800 nm. Evidently, the absorption in 700–800 nm on CuO<sub>x</sub>-rutile and CuO<sub>x</sub>-anatase stems from the d-d excitation of CuO<sub>x</sub> [28]. The absorption of 420–500 nm on CuO<sub>x</sub>-rutile should not originate from the individual excitation of TiO<sub>2</sub> or CuO<sub>x</sub>, and it may be caused by direct charge transfer from valance band of rutile TiO<sub>2</sub> to CuO<sub>x</sub> nanoparticle (see below for more discussion). Other optical properties such as photocurrent and EIS were also measured. Consistent

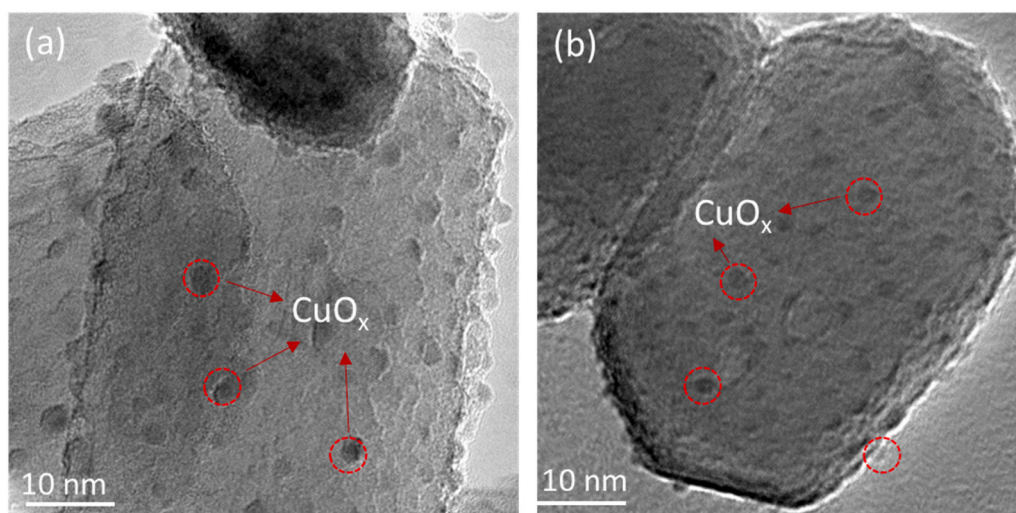


Fig. 3. The TEM image of CuO<sub>x</sub>-rutile (a) and CuO<sub>x</sub>-anatase (b).

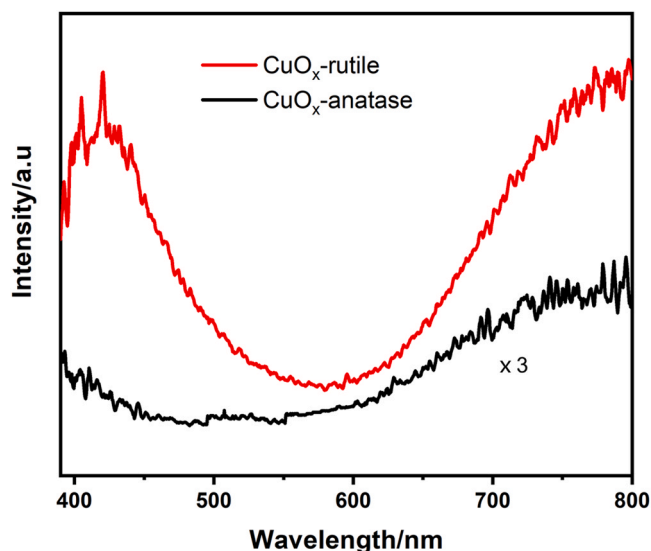


Fig. 4. UV-vis diffuse reflectance spectra of  $\text{CuO}_x$ -rutile and  $\text{CuO}_x$ -anatase with rutile and anatase as background, respectively.

with the results about activity tests, the  $\text{CuO}_x$ -rutile possesses higher photocurrents and the lower electrochemical impedances, compared with  $\text{CuO}_x$ -anatase under visible light irradiation (Figs. S10 and S11). In contrast,  $\text{CuO}_x$ -rutile possesses lower photocurrents and the higher electrochemical impedances compared with  $\text{CuO}_x$ -anatase under UV irradiation (Figs. S12 and S13). These findings further suggest that  $\text{CuO}_x$ -rutile and  $\text{CuO}_x$ -anatase may have completely different photoexcitation pathway under visible light.

### 3.4. Mechanism discussion of charge migration on $\text{CuO}_x$ - $\text{TiO}_2$

As reported, the decomposition of model organic pollutants is frequently used to judge the efficiency of  $\text{CuO}_x$ - $\text{TiO}_2$ , for instance, the  $\text{CuO}_x$ - $\text{TiO}_2$  or  $\text{FeO}_x$ - $\text{TiO}_2$  shows excellent activities for oxidation of acetone and degradation of 2-naphthol or other dyes [13,29–34]. Since the active species such as holes, electrons,  $\cdot\text{O}_2^-$ , and  $\cdot\text{OH}$  are all involved in these reactions, the specific role and source of the hole cannot be determined. Previous studies and our recent reports have confirmed that  $\text{NH}_3$  oxidation is a hole-position sensitive reaction, and the activation of  $\text{NH}_3$  by hole into  $\text{NH}_2$  radical is the activity-determining step [22–24],

which means that an active visible-light photocatalyst for  $\text{NH}_3$  oxidation should have a low valence band (VB) edge with high oxidation potential. For instance, semiconductor with low VB position, such as  $\text{TiO}_2$ ,  $\text{Ag}_3\text{PO}_4$ , and  $\text{WO}_3$ , is able to oxidize  $\text{NH}_3$  when they are photoexcited under suitable irradiation [23]. The distinct performances in  $\text{NH}_3$  oxidation between  $\text{CuO}_x$ -rutile and  $\text{CuO}_x$ -anatase suggest that visible light might excites electrons from VB of rutile to the  $\text{CuO}_x$ , then holes in VB of rutile  $\text{TiO}_2$  are capable of oxidizing  $\text{NH}_3$ . By contrast, visible light might only excite electrons from VB of  $\text{CuO}_x$  to CB of  $\text{CuO}_x$  on anatase  $\text{TiO}_2$ , then holes in VB of  $\text{CuO}_x$  cannot oxidize  $\text{NH}_3$ .

EPR is a powerful tool to detect the photo-excited holes and electrons of  $\text{TiO}_2$  and to investigate the chemical changes of  $\text{CuO}_x$  species under UV or visible light irradiation [7,16,28]. Fig. 5 show that the EPR signals of  $\text{Cu}^{2+}$  in  $\text{CuO}_x$ -rutile and  $\text{CuO}_x$ -anatase became broader in the dark, probably due to the inhomogeneity of the chemical structure surrounding  $\text{Cu}^{2+}$  ions. Upon visible light irradiation, the  $\text{Cu}^{2+}$  signal decrease in the case of the  $\text{CuO}_x$ -rutile, and a small signal at  $g = 2.010$  ascribed to trapped holes in the VB of  $\text{TiO}_2$  is observed. The similar signal is also observed under UV irradiation. However, the  $\text{Cu}^{2+}$  signal in  $\text{CuO}_x$ -anatase has no changes upon visible light irradiation, and no signal of trapped holes is observed. When the visible light was switched to UV irradiation, the  $\text{Cu}^{2+}$  signal on anatase decrease and the signals of trapped holes appear. The decrease of  $\text{Cu}^{2+}$  signal is associated with the appearance of trapped holes, corresponding to the excited electrons from the VB of  $\text{TiO}_2$  to the surface of  $\text{CuO}_x$ . Hence, we confirm that on the interface of  $\text{CuO}_x$  and rutile  $\text{TiO}_2$ , electrons are excited from VB of rutile  $\text{TiO}_2$  to the  $\text{CuO}_x$  under visible light, while in case of the surface of  $\text{CuO}_x$  and anatase  $\text{TiO}_2$ , the VB electrons of anatase  $\text{TiO}_2$  are not excited under visible light irradiation.

The different photocatalytic charge separation process in semiconductors would induce the formation of distinct reactive species, such as hydroxyl radical ( $\cdot\text{OH}$ ) and superoxide radical ( $\cdot\text{O}_2^-$ ), etc. [35,36]. We next measured the related active species on  $\text{CuO}_x$ -rutile and  $\text{CuO}_x$ -anatase under visible light. Fig. 6a show that 4 strong characteristic peaks of the DMPO- $\cdot\text{OH}$  adducts appear in  $\text{CuO}_x$ -rutile under visible light, while the DMPO- $\cdot\text{OH}$  adducts signal of  $\text{Cu}$ -anatase is very weak under same conditions, indicating that the large amount of  $\cdot\text{OH}$  species are formed on  $\text{CuO}_x$ -rutile, but it is extremely low on  $\text{CuO}_x$ -anatase. The  $\cdot\text{O}_2^-$  species are typical radicals through activating  $\text{O}_2$  molecules by the photoexcited electrons [37,38], and the DMPO- $\cdot\text{O}_2^-$  species in acetonitrile dispersions were also measured under visible light irradiation (Fig. 6b). Both  $\text{CuO}_x$ -rutile and  $\text{CuO}_x$ -anatase has strong DMPO- $\cdot\text{O}_2^-$  species signal, indicating electrons from CB of  $\text{CuO}_x$  or CB of anatase

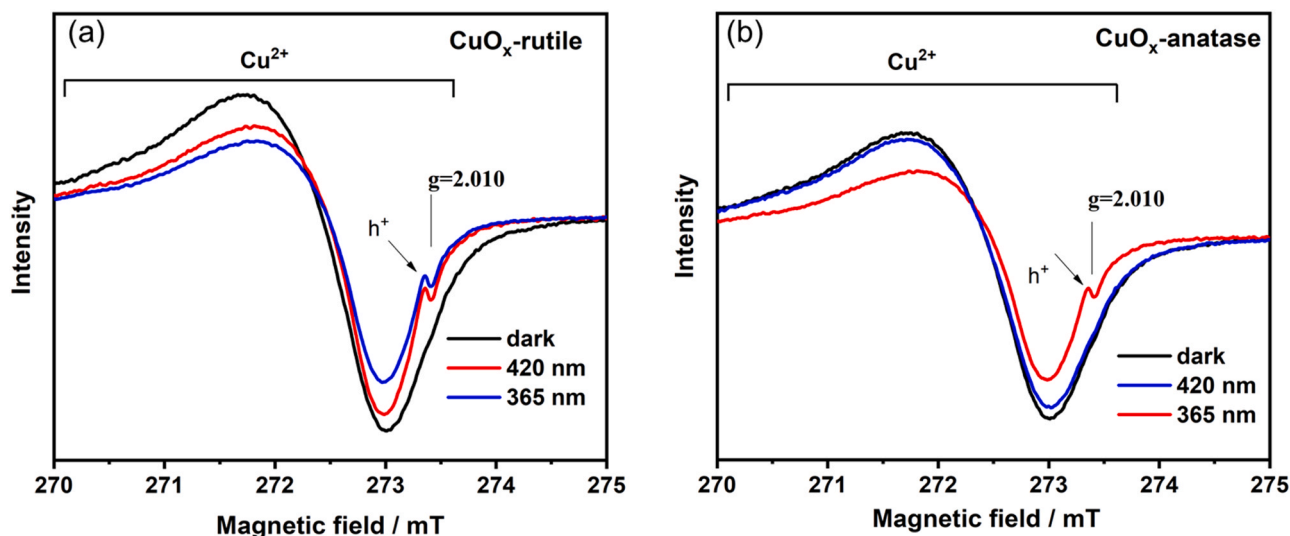


Fig. 5. EPR spectra of  $\text{CuO}_x$ -rutile (a) and  $\text{CuO}_x$ -anatase (b) measured at 77 K under vacuum with visible light or UV irradiation.

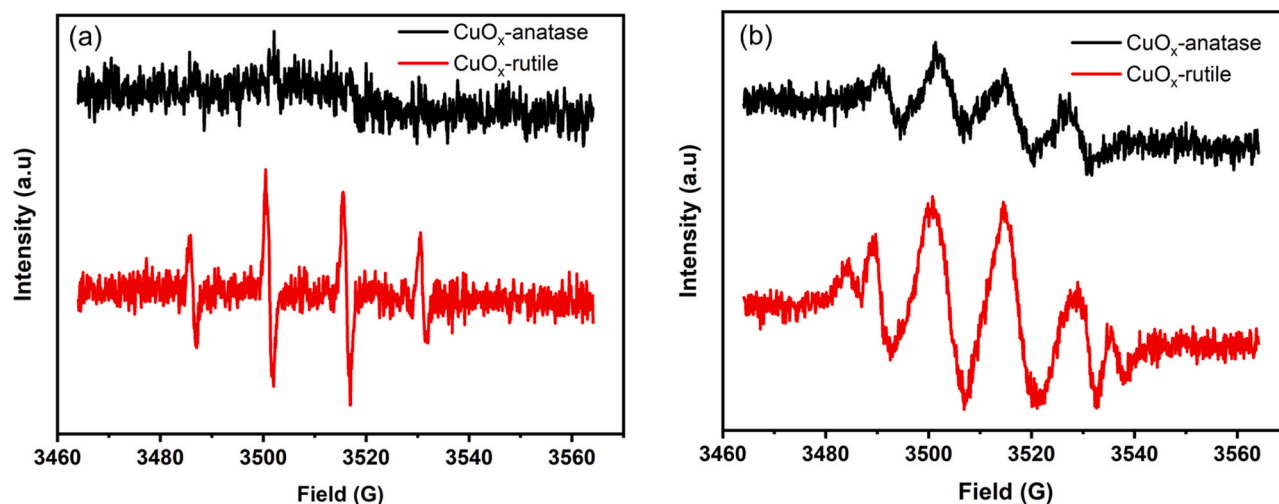


Fig. 6. DMPO spin-trapping EPR spectra measured at 303 K after 5 min visible irradiation in aqueous solutions (a) and acetonitrile (b) over different samples.

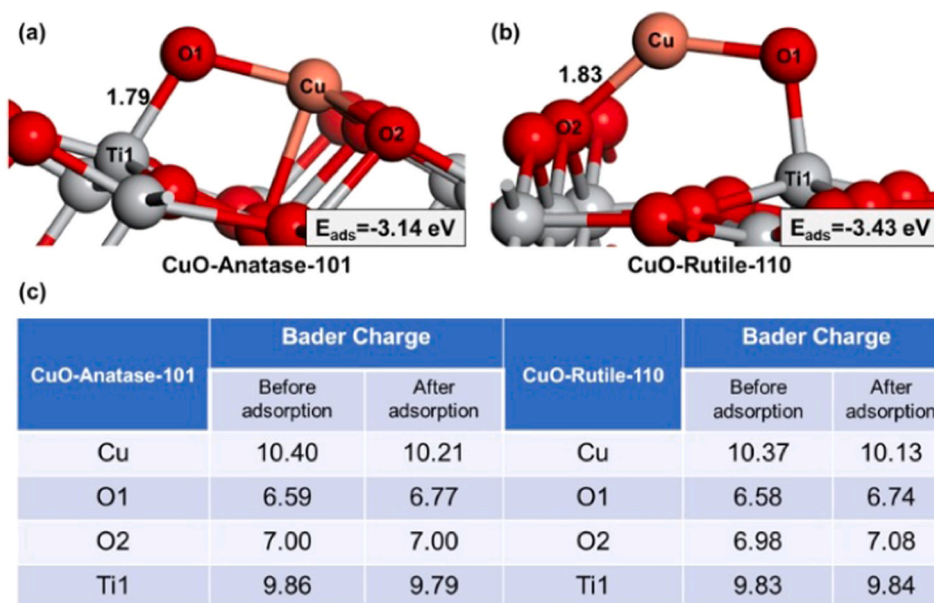


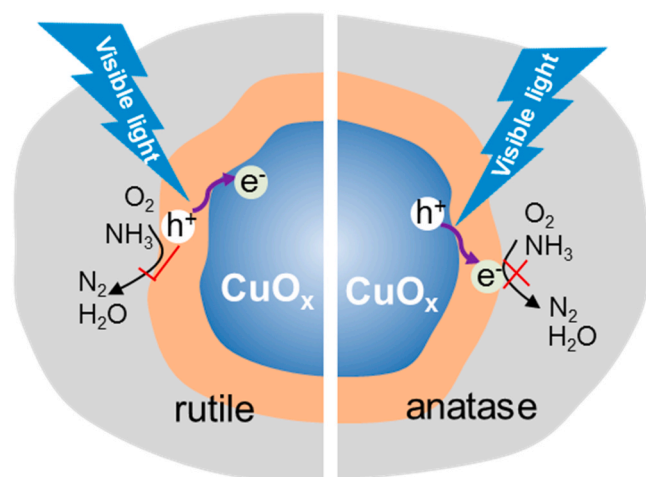
Fig. 7. The optimization structures of CuO-anatase-101 and CuO-rutile-110 (a, b) and Bader charge before and after CuO adsorbed on anatase and rutile (c).

TiO<sub>2</sub> all can efficiently activate O<sub>2</sub>. The results of DMPO-·OH adducts and DMPO-·O<sub>2</sub><sup>-</sup> adducts further reveal that the sources of excited hole are different on the CuO<sub>x</sub>-rutile and CuO<sub>x</sub>-anatase under visible light. The holes on CuO<sub>x</sub>-rutile are from the low VB of TiO<sub>2</sub>, and it is capable of producing the ·OH radicals. In contrast, the holes on CuO<sub>x</sub>-anatase are from the VB of CuO<sub>x</sub>, and it can not oxidize the H<sub>2</sub>O to ·OH radicals.

DFT calculations were next carried out to further explore why charge separation process greatly depend on the crystalline structure of the TiO<sub>2</sub>. Fig. 7 presents the optimization structures of CuO-anatase-101 and CuO-rutile-110. It is shown that Cu atom in CuO is bonded with the surface bridge oxygen (O2) of TiO<sub>2</sub>, and O1 in CuO is bonded with Ti1 in both CuO-anatase-101 and CuO-rutile-110 interfaces. The interfacial Cu—O2 and Ti1—O1 bonds between CuO and anatase-101 surface have a distance of 2.02 Å and 1.79 Å, while Cu—O2 and Ti—O1 bond between CuO and rutile-110 surface have a distance of 1.83 Å and 1.75 Å. The adsorption energy between CuO<sub>x</sub> and different crystalline TiO<sub>2</sub> was then calculated. The adsorption energy is -3.14 eV and -3.43 eV for CuO adsorption on anatase and rutile TiO<sub>2</sub>, respectively (Fig. 4a), indicating that the interaction between CuO<sub>x</sub> and rutile TiO<sub>2</sub> is stronger

than that of CuO<sub>x</sub> and anatase TiO<sub>2</sub>. The Bader charge was further analyzed, and the results are shown in Fig. 4c. When CuO is adsorbed on anatase-101 surface, the Bader charge of interfacial Ti1 is reduced from 9.86 to 9.79, while the Bader charge of the surface bridge oxygen shows no significant change, indicating that the interaction between CuO and anatase TiO<sub>2</sub> should occur in the interfacial Ti and the oxygen in CuO<sub>x</sub>. Hence, the interfacial charge transfer between CuO and anatase TiO<sub>2</sub> should occur in the interfacial Ti and the oxygen in CuO<sub>x</sub>, specifically, visible light inclines to drive the electrons of interfacial O in CuO<sub>x</sub> to the interfacial Ti in anatase-101. Interestingly, in case of CuO-rutile-110, the Bader charge of interfacial Ti has no significant change after CuO adsorb on rutile-110, while the Bader charge of the surface bridge oxygen is increased from 6.98 to 7.08, indicating that the interaction between CuO and rutile TiO<sub>2</sub> mainly stems from the interaction of surface bridge oxygen and interfacial Cu in CuO<sub>x</sub>. Therefore, the charge transfer in CuO-rutile-110 takes place in a opposite mode compared with that of CuO-anatase-101, that the visible light inclines to drive the electrons of surface bridge O in rutile-110 to the interfacial Cu in CuO<sub>x</sub>.

The strong interaction between noble metal and metal oxide, such as



**Scheme 1.** Charge separation processes in  $\text{CuO}_x$ -rutile and  $\text{CuO}_x$ -anatase.

Au, Pt and Pd supported on  $\text{TiO}_2$ ,  $\text{FeO}_x$  and  $\text{CeO}_2$ , etc. [39–42], has been widely investigated in the field of catalysis, and it is shown to greatly influence the catalytic activity and selectivity. Additionally, the interface of metal and oxide has been also identified as active site in catalytic oxidation or reduction reactions [43–45]. Our present results show that the interaction between  $\text{MO}_x$  and  $\text{TiO}_2$  is also the key factor determining the direction of charge transfer in  $\text{CuO}_x$ - $\text{TiO}_2$ . Since the interactions between  $\text{CuO}_x$  and  $\text{TiO}_2$  in  $\text{CuO}_x$ -anatase and  $\text{CuO}_x$ -rutile are much different from each other, the electronic distributions of interfacial Cu, O and Ti atoms are markedly different, and then inducing the distinct direction of charge transfer.

#### 4. Conclusions

In summary, by using a hole-position sensitive  $\text{NH}_3$  oxidation as probe reaction, we found a usual photocatalytic phenomenon that  $\text{CuO}_x$ -anatase shows better activity than the  $\text{CuO}_x$ -rutile under UV, and an unusual phenomenon that  $\text{CuO}_x$ -rutile shows activity, while no activity was observed on  $\text{CuO}_x$ -anatase under visible light. In combination with EPR and DFT calculations, we discovered that the crystalline forms of  $\text{TiO}_2$  remarkably influence the charge separation of  $\text{CuO}_x$ - $\text{TiO}_2$  due to the different interactions between  $\text{CuO}_x$  and  $\text{TiO}_2$  in  $\text{CuO}_x$ -anatase and  $\text{CuO}_x$ -rutile, resulting in the distinct direction of charge transfer. The detailed processes of charge separation are presented in Scheme 1. On the interface of  $\text{CuO}_x$  and rutile  $\text{TiO}_2$ , the electrons of rutile  $\text{TiO}_2$  are transferred from VB directly to the  $\text{CuO}_x$  under visible light irradiation. Due to the low VB position of  $\text{TiO}_2$ , the left holes have high oxidation potential and therefore could efficiently oxidize  $\text{NH}_3$ . On the interface of  $\text{CuO}_x$  and anatase  $\text{TiO}_2$ , visible light irradiation can only drive the excitation of  $\text{CuO}_x$  itself. The left holes of  $\text{CuO}_x$  have low oxidation potential and therefore cannot oxidize  $\text{NH}_3$  due to the high VB position of  $\text{CuO}_x$ . This work provides a facile probe oxidation reaction to intensively study the mechanism of charge migration in  $\text{CuO}_x$ - $\text{TiO}_2$  and the findings will contribute to a deeper understanding of the basic photocatalytic process.

#### CRediT authorship contribution statement

**Min Chen:** Conceptualization, Methodology, Validation, Formal analysis, Investigation, Resources, Data curation, Visualization, Writing – original draft, Writing – review & editing. **Jianhua Chen:** Investigation, Resources, Data curation. **Chuncheng Chen:** Formal analysis, Investigation, Writing – original draft. **Changbin Zhang:** Writing – original draft, Writing – review & editing, Supervision, Project administration, Funding acquisition. **Hong He:** Supervision, Project administration.

#### Declaration of Competing Interest

The authors declare that they have no known competing financial interests or personal relationships that could have appeared to influence the work reported in this paper.

#### Acknowledgements

This work was financially supported by the National Key Research and Development Program of China (2017YFC0211802) and the National Natural Science Foundation of China (21906174, 22025604, 21976196).

#### Appendix A. Supporting information

Supplementary data associated with this article can be found in the online version at doi:10.1016/j.apcatb.2021.120735.

#### References

- [1] A. Fujishima, X.T. Zhang, D.A. Tryk,  $\text{TiO}_2$  photocatalysis and related surface phenomena, *Surf. Sci. Rep.* 63 (2008) 515–582.
- [2] H. Xu, S. Ouyang, L. Liu, P. Reunchan, N. Umezawa, J. Ye, Recent advances in  $\text{TiO}_2$ -based photocatalysis, *J. Mater. Chem. A* 2 (2014) 12642–12661.
- [3] R. Asahi, T. Morikawa, H. Irie, T. Ohwaki, Nitrogen-doped titanium dioxide as visible-light-sensitive photocatalyst: designs, developments, and prospects, *Chem. Rev.* 114 (2014) 9824–9852.
- [4] J. Low, B. Cheng, J. Yu, Surface modification and enhanced photocatalytic  $\text{CO}_2$  reduction performance of  $\text{TiO}_2$ : a review, *Appl. Surf. Sci.* 392 (2017) 658–686.
- [5] S. Zhu, X.F. Chen, Z.C. Li, X.Y. Ye, Y. Liu, Y. Chen, L. Yang, M. Chen, D.Q. Zhang, G. S. Li, H.X. Li, Cooperation between inside and outside of  $\text{TiO}_2$ : lattice  $\text{Cu}^+$  accelerates carrier migration to the surface of metal copper for photocatalytic  $\text{CO}_2$  reduction, *Appl. Catal. B: Environ.* 264 (2020), 118515.
- [6] D.W. Ni, H.Y. Shen, H.Q. Li, Y. Ma, T.Y. Zhai, Synthesis of high efficient  $\text{Cu}/\text{TiO}_2$  photocatalysts by grinding and their size-dependent photocatalytic hydrogen production, *Appl. Surf. Sci.* 409 (2017) 241–249.
- [7] N. Seriani, C. Pinilla, Y. Crespo, Presence of gap states at  $\text{Cu}/\text{TiO}_2$  anatase surfaces: consequences for the photocatalytic activity, *J. Phys. Chem. C* 119 (2015) 6696–6702.
- [8] K. Osako, K. Matsuzaki, T. Susaki, S. Ueda, G. Yin, A. Yamaguchi, H. Hosono, M. Miyauchi, Direct observation of interfacial charge transfer between rutile  $\text{TiO}_2$  and ultrathin  $\text{CuO}_x$  film by visible-light illumination and its application for efficient photocatalysis, *Chemcatchem* 10 (2018) 3666–3670.
- [9] A. Suligoj, I. Arcon, M. Mazaj, G. Dražić, D. Arcon, P. Cool, U.L. Štangar, N. N. Tušar, Surface modified titanium dioxide using transition metals: nickel as a winning transition metal for solar light photocatalysis, *J. Mater. Chem. A* 6 (2018) 9882–9892.
- [10] P. Unwiset, A. Makdee, K.C. Chanapattarapol, P. Kidkhunthod, Effect of Cu addition on  $\text{TiO}_2$  surface properties and photocatalytic performance: X-ray absorption spectroscopy analysis, *J. Phys. Chem. Solids* 120 (2018) 231–240.
- [11] Y. Ide, N. Inami, H. Hattori, K. Saito, M. Sohmiya, N. Tsunoi, K. Komaguchi, T. Sano, Y. Bando, D. Golberg, Y. Sugahara, Remarkable charge separation and photocatalytic efficiency enhancement through interconnection of  $\text{TiO}_2$  nanoparticles by hydrothermal treatment, *Angew. Chem. Int. Ed.* 55 (2016) 3600–3605.
- [12] G. Xiang, Y.G. Wang, D. Wu, T. Li, J. He, J. Li, X. Wang, Size-dependent surface activity of rutile and anatase  $\text{TiO}_2$  nanocrystals: facile surface modification and enhanced photocatalytic performance, *Chemistry* 18 (2012) 4759–4765.
- [13] H. Irie, K. Kamiya, T. Shibamura, S. Miura, D.A. Tryk, T. Yokoyama, K. Hashimoto, Visible light-sensitive Cu (II)-grafted  $\text{TiO}_2$  photocatalysts: activities and X-ray absorption fine structure analyses, *J. Phys. Chem. C* 113 (2009) 10761–10766.
- [14] D. Wang, X.Y. Pan, G.T. Wang, Z.G. Yi, Improved propane photooxidation activities upon nano  $\text{Cu}_2\text{O}/\text{TiO}_2$  heterojunction semiconductors at room temperature, *RSC Adv.* 5 (2015) 22038–22043.
- [15] M.V. Dozzi, G.L. Chiarello, M. Pedroni, S. Livraghi, E. Giamello, E. Selli, High photocatalytic hydrogen production on Cu (II) pre-grafted  $\text{Pt}/\text{TiO}_2$ , *Appl. Catal. B* 209 (2017) 417–428.
- [16] Y. Nosaka, S. Takahashi, H. Sakamoto, A.Y. Nosaka, Reaction mechanism of Cu (II)-grafted visible-light responsive  $\text{TiO}_2$  and  $\text{WO}_3$  photocatalysts studied by means of ESR spectroscopy and chemiluminescence photometry, *J. Phys. Chem. C* 115 (2011) 21283–21290.
- [17] Q. Jin, M. Fujishima, A. Iwaszuk, M. Nolan, H. Tada, Loading effect in copper (II) oxide cluster-surface-modified titanium (IV) oxide on visible- and UV-light activities, *J. Phys. Chem. C* 117 (2013) 23848–23857.
- [18] D. Zhang, Y.L. Guo, Z.K. Zhao, Porous defect-modified graphitic carbon nitride via a facile one-step approach with significantly enhanced photocatalytic hydrogen evolution under visible light irradiation, *Appl. Catal. B* 226 (2018) 1–9.
- [19] J. Yu, S. Wang, J. Low, W. Xiao, Enhanced photocatalytic performance of direct Z-scheme  $g\text{-C}_3\text{N}_4\text{-TiO}_2$  photocatalysts for the decomposition of formaldehyde in air, *Phys. Chem. Chem. Phys.* 15 (2013) 16883–16890.

- [20] C.C. Chen, W.H. Ma, J.C. Zhao, Semiconductor-mediated photodegradation of pollutants under visible-light irradiation, *Chem. Soc. Rev.* 39 (2010) 4206–4219.
- [21] M. Liu, X. Qiu, M. Miyauchi, K. Hashimoto, Energy-level matching of Fe (III) ions grafted at surface and doped in bulk for efficient visible-light photocatalysts, *J. Am. Chem. Soc.* 135 (2013) 10064–10072.
- [22] M. Chen, J.Z. Ma, B. Zhang, G.Z. He, Y.B. Li, C.B. Zhang, H. He, Remarkable synergistic effect between {001} facets and surface F ions promoting hole migration on anatase TiO<sub>2</sub>, *Appl. Catal. B* 207 (2017) 397–403.
- [23] M. Chen, C. Zhang, H. He, Insights into designing photocatalysts for gaseous ammonia oxidation under visible light, *Environ. Sci. Technol.* 54 (2020) 10544–10550.
- [24] M. Chen, J.Z. Ma, B. Zhang, F. Wang, Y.B. Li, C.B. Zhang, H. He, Facet-dependent performance of anatase TiO<sub>2</sub> for photocatalytic oxidation of gaseous ammonia, *Appl. Catal. B* 223 (2018) 209–215.
- [25] G.Q. Cao, N.A. Deskins, N. Yi, Chemical source profiles of particulate matter and gases emitted from solid fuels for residential cooking and heating scenarios in Qinghai-Tibetan Plateau, *Environ. Pollut.* 285 (2021), 117503.
- [26] Y.J. Kim, J.K. Lee, K.M. Min, S.B. Hong, I.-S. Nam, B.K. Cho, Hydrothermal stability of CuSSZ-13 for reducing NO<sub>x</sub> by NH<sub>3</sub>, *J. Catal.* 311 (2014) 447–457.
- [27] L. Liu, F. Gao, H. Zhao, Y. Li, Tailoring Cu valence and oxygen vacancy in Cu/TiO<sub>2</sub> catalysts for enhanced CO<sub>2</sub> photoreduction efficiency, *Appl. Catal. B* 134–135 (2013) 349–358.
- [28] M. Jung, J.N. Hart, J. Scott, Y.H. Ng, Y. Jiang, R. Amal, Exploring Cu oxidation state on TiO<sub>2</sub> and its transformation during photocatalytic hydrogen evolution, *Appl. Catal. A* 521 (2016) 190–201.
- [29] M.H. Jeong, J. Sun, G.Y. Han, D.H. Lee, J.W. Bae, Successive reduction-oxidation activity of FeO<sub>x</sub>/TiO<sub>2</sub> for dehydrogenation of ethane and subsequent CO<sub>2</sub> activation, *Appl. Catal. B: Environ.* 270 (2020), 118887.
- [30] H. Zhang, W. Wang, H. Zhao, L. Zhao, L.-Y. Gan, L.-H. Guo, Facet-dependent interfacial charge transfer in Fe (III)-grafted TiO<sub>2</sub> nanostructures activated by visible light, *ACS Catal.* 8 (2018) 9399–9407.
- [31] H. Yu, H. Irie, Y. Shimodaira, Y. Hosogi, Y. Kuroda, M. Miyauchi, K. Hashimoto, An efficient visible-light-sensitive Fe (III)-grafted TiO<sub>2</sub> photocatalyst, *J. Phys. Chem. C* 114 (2010) 16481–16487.
- [32] X. Qiu, M. Miyauchi, H. Yu, H. Irie, K. Hashimoto, Visible-light-driven Cu (II)-(Sr<sub>1-y</sub>Na<sub>y</sub>)(Ti<sub>1-x</sub>Mo<sub>x</sub>)O<sub>3</sub> photocatalysts based on conduction band control and surface ion modification, *J. Am. Chem. Soc.* 132 (2010) 15259–15267.
- [33] Y. Li, W.-N. Wang, Z. Zhan, M.-H. Woo, C.-Y. Wu, P. Biswas, Photocatalytic reduction of CO<sub>2</sub> with H<sub>2</sub>O on mesoporous silica supported Cu/TiO<sub>2</sub> catalysts, *Appl. Catal. B* 100 (2010) 386–392.
- [34] N. Murakami, T. Chiyoya, T. Tsubota, T. Ohno, Switching redox site of photocatalytic reaction on titanium (IV) oxide particles modified with transition-metal ion controlled by irradiation wavelength, *Appl. Catal. A* 348 (2008) 148–152.
- [35] S.L. Wang, X. Luo, X. Zhou, Y. Zhu, X. Chi, W. Chen, K. Wu, Z. Liu, S.Y. Quek, G. Q. Xu, Fabrication and properties of a free-standing two-dimensional titania, *J. Am. Chem. Soc.* 139 (2017) 15414–15419.
- [36] S.-J. Yuan, J.-J. Chen, Z.-Q. Lin, W.-W. Li, G.-P. Sheng, H.-Q. Yu, Nitrate formation from atmospheric nitrogen and oxygen photocatalysed by nano-sized titanium dioxide, *Nat. Commun.* 4 (2013) 2249.
- [37] M. D'Arienzo, J. Carbajo, A. Bahamonde, M. Crippa, S. Polizzi, R. Scotti, L. Wahba, F. Morazzoni, Photogenerated defects in shape-controlled TiO<sub>2</sub> anatase nanocrystals: a probe to evaluate the role of crystal facets in photocatalytic processes, *J. Am. Chem. Soc.* 133 (2011) 17652–17661.
- [38] M.M. Montemore, M.A. van Spronsen, R.J. Madix, C.M. Friend, O<sub>2</sub> activation by metal surfaces: implications for bonding and reactivity on heterogeneous catalysts, *Chem. Rev.* 118 (2018) 2816–2862.
- [39] J. Resasco, L. DeRita, S. Dai, J.P. Chada, M. Xu, X. Yan, J. Finzel, S. Hanukovich, A. S. Hoffman, G.W. Graham, S.R. Bare, X. Pan, P. Christopher, Uniformity is key in defining structure-function relationships for atomically dispersed metal catalysts: the case of Pt/CeO<sub>2</sub>, *J. Am. Chem. Soc.* 142 (2020) 169–184.
- [40] B. Han, Y. Guo, Y. Huang, W. Xi, J. Xu, J. Luo, H. Qi, Y. Ren, X. Liu, B. Qiao, T. Zhang, Strong metal-support interactions between Pt single atoms and TiO<sub>2</sub>, *Angew. Chem. Int. Ed.* 59 (2020) 11824–11829.
- [41] H. Wang, J.X. Liu, L.F. Allard, S. Lee, J. Liu, H. Li, J. Wang, J. Wang, S.H. Oh, W. Li, M. Flytzani-Stephanopoulos, M. Shen, B.R. Goldsmith, M. Yang, Surpassing the single-atom catalytic activity limit through paired Pt-O-Pt ensemble built from isolated Pt1 atoms, *Nat. Commun.* 10 (2019) 3808.
- [42] D. Kunwar, S. Zhou, A. DeLaRiva, E.J. Peterson, H. Xiong, X.I. Pereira-Hernández, S.C. Purdy, R. ter Veen, H.H. Brongersma, J.T. Miller, H. Hashiguchi, L. Kovarik, S. Lin, H. Guo, Y. Wang, A.K. Datye, Stabilizing high metal loadings of thermally stable platinum single atoms on an industrial catalyst support, *ACS Catal.* 9 (2019) 3978–3990.
- [43] M. Cargnello, V.V. Doan-Nguyen, T.R. Gordon, R.E. Diaz, E.A. Stach, R.J. Gorte, P. Fornasiero, C.B. Murray, Control of metal nanocrystal size reveals metal-support interface role for ceria catalysts, *Science* 341 (2013) 771–773.
- [44] G. Chen, Y. Zhao, G. Fu, P.N. Duchesne, L. Gu, Y. Zheng, X. Weng, M. Chen, P. Zhang, C.W. Pao, J.F. Lee, N. Zheng, Interfacial effects in iron-nickel hydroxide-platinum nanoparticles enhance catalytic oxidation, *Science* 344 (2014) 495–499.
- [45] Y.-Q. Su, Y. Wang, J.-X. Liu, I.A.W. Filot, K. Alexopoulos, L. Zhang, V. Muravev, B. Zijlstra, D.G. Vlachos, E.J.M. Hensen, Theoretical approach to predict the stability of supported single-atom catalysts, *ACS Catal.* 9 (2019) 3289–3297.